Comparison of Traction Controllers for Electric Vehicles With On-Board Drivetrains

Comparison of Traction Controllers for Electric Vehicles with On-Board Drivetrains

Stefano De Pinto, Christoforos Chatzikomis, Aldo Sorniotti, *Member*, *IEEE*, Giacomo Mantriota

***Abstract*—An extensive literature discusses traction control systems for electric vehicles. In general, the proposed control structures do not include consideration of the actuation dynamics, which are especially important for vehicles with on-board drivetrains, usually characterized by significant torsional dynamics of the half-shafts. This paper compares the performance of a selection of traction controllers from the literature with control structures specifically designed for on-board electric drivetrains. The simulation results clearly show the performance improvement provided by the control structures taking into account the actuation dynamics.**

***Index Terms*—Fully electric vehicle; traction control; on-board drivetrain; PID control; H∞ control; sliding mode control**

I. List of symbols

a: longitudinal acceleration
$A_s(v), B_s(v), C_s(v)$: shaped plant matrices, functions of vehicle speed
b: coefficient of the first order sliding mode controller
c_λ: longitudinal slip stiffness
C_{drag}: aerodynamic drag coefficient
e: error
f_0, f_2: constant and quadratic coefficient of the rolling resistance force
F: force
g: acceleration of gravity
G: transfer function
GM: gain margin
h: index used for the gain scheduling points
H: height of the centre of gravity of the vehicle
$H_s(v), F_s(v)$: output of the H_∞ optimization procedure , functions of vehicle speed
i_1, i_2: transmission gear ratios
I: identity matrix
J: mass moment of inertia
k: torsional stiffness
K: gain
L: wheelbase
L_{tire}: tire relaxation length
M: mass of the vehicle
PM: phase margin
R: radius
s: Laplace operator
S: frontal area of the vehicle
T: torque
u: control input
$v, \dot{v}$: vehicle speed and acceleration
V: Lyapunov function
W: shaped plant used in the H_∞ observer based form
x: state variables in the state space approach
y: output in the state space approach
α: parameter used in the MTTE controller
β: torsional damping coefficient
γ: upper bound of the sliding mode controllers
Γ: uncertain term of the SOSM, function of the states and time
ϵ: stability margin
η: efficiency
$\vartheta, \dot{\vartheta}, \ddot{\vartheta}$: angular position, speed, acceleration
λ: slip ratio
μ: road friction coefficient
ν: derivative of the control input u
ρ: air density
σ: sliding variable
τ: time constant delay
φ: value for the H_∞ optimization procedure
Φ: uncertain term of the SOSM, function of the states, input and time
χ: gain used in the MTTE controller
Ω: equivalent control in the friction estimation through sliding mode

The following superscripts and subscripts are used in the paper:
act: actual
aer: aerodynamic
AVC: active vibration controller
bp: break point
d: delayed
eq: equivalent
f, r: front, rear
fin: final
g: gear
HS: half-shaft
in: initial
I: integral term
m: motor
man: manoeuvre
max: maximum
MTTE: maximum transmissible torque estimation
P: proportional term
ref: reference
$roll$: rolling resistance
SMC: sliding mode controller
$SOSM$: sub-optimal sliding mode
TC: traction controller
w: wheel

II. Introduction

Electric vehicles (EVs) with multiple and individually controlled drivetrains present significant potential benefits with respect to more conventional EV layouts with a single electric drivetrain, an open differential and half-shafts. In fact, these vehicle configurations can produce torque-vectoring, which is yaw moment control actuated through the torque difference among the left and right wheels of the same axle. Torque-vectoring significantly improves the vehicle cornering response, thus enhancing active safety. For example, torque-vectoring increases the maximum lateral acceleration in steady-state conditions, and yaw damping during transients [1]-[2].

Moreover, the continuous control of the individual drivetrain torque levels can provide improved slip ratio tracking performance during extreme traction or braking, with respect to conventional internal-combustion-engine-driven vehicles. Hence, the performance of traction controllers (TC) and anti-lock braking systems (ABS) can be enhanced by the adoption of electric drivetrains. In fact, electric motor drives are characterized by more precise and fast torque response, with respect to internal combustion engines or hydraulic friction brakes. Therefore, they are more suitable for continuous wheel slip control.

An extensive literature describes traction control (TC) systems, or more generally wheel slip controllers, potentially suitable for EVs with multiple drivetrains. These control structures range from controllers not requiring the definition of a reference slip ratio [4], to controllers based on slip ratio feedback control. The feedback control action can be based on gain scheduled proportional integral derivative (PID) control structures [], H_∞ controllers [], sliding mode controllers [], and model predictive controllers [].

More specifically, the proposed controllers are usually based on the simplified equations of the wheel dynamics, with the slip ratio used as a state. They exclude consideration of: i) tyre relaxation [], which is very relevant according to industrial sources []; and ii) drivetrain torsional dynamics, which can provoke a significant deviation between the expected and the actual wheel torque, according to simulation and experimental studies []. This is an important limitation, as the on-board (rather than the in-wheel) installation of the electric drivetrains is the preferred solution in many applications, mainly for packaging constraints.

The novel contributions of this paper are:

- The analysis of the variation of the system dynamic response, when considering tyre relaxation and drivetrain torsional dynamics for traction control design.
- The development of PID and H_∞ controllers specifically designed for wheel slip control with on-board electric drivetrains.
- The objective comparison of the performance of different control structures from the literature, with that of the novel traction controllers designed in this paper. Among the controllers from the literature, this paper focuses on the PID controllers, a couple sliding mode control formulations, and the maximum transmissible torque estimation controller.

The paper is structured as follows. Section III describes the models for control system design. Section IV presents the formulations of the control structures that will be the object of the comparison in Section V. Section VI includes the main conclusions of the research.

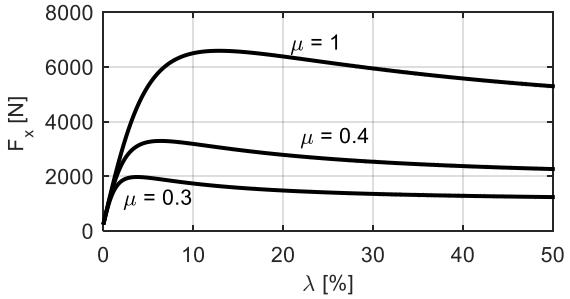

Fig.1. Longitudinal tire force as function of the slip ratio for different values of the tire-road friction coefficient μ, for $F_z = 6130$ N.

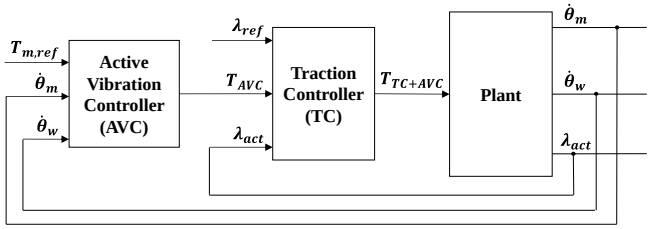

Fig.2. Scheme of the proposed Traction controller (TC) and active vibration controller (AVC).

III. Design requirements

Fig. 1 shows a typical longitudinal force (F_x) – slip ratio (λ) characteristic of a passenger car tire, for different values of the tire-road friction coefficient μ. The value of λ that maximizes the longitudinal force is a function of μ. Actual traction controllers include algorithms for the estimation of μ []. However, these are usually very approximate, and in real-world applications the friction coefficient is often estimated according to two or three discrete levels. Also, the shape of the $F_x(\lambda)$ characteristic can be very different depending on μ, e.g., it can happen that F_x is monotonically increasing as a function of λ, or that the slip ratio corresponding to the maximum value of F_x is very different from the expected one. As a consequence of the actual tire characteristics, the first essential requirement of any TC is to be able to operate for a wide range of values of the local longitudinal slip stiffness, c_λ. This is defined as:

$$c_\lambda = \left.\frac{\partial F_x}{\partial \lambda}\right|_{\lambda=\lambda_{act}} \tag{1}$$

The second requirement is that the TC is operational only when strictly required, i.e., to limit $|\lambda|$ when its estimated value is above specified thresholds. During its interventions, the TC outputs a torque correction, i.e., a reduction (and never an increase) of the electric motor torque with respect to the value produced by the low-level layer of the torque-vectoring controller. The TC must be de-activated when the slip ratio is back within its normal values. Therefore, the control structure

has to be flexible enough to allow ease of activation/deactivation in a limited time frame. Thirdly, the control action should be as smooth as possible, to allow comfortable vehicle operation, and not to provoke accelerated wear of the electric drivetrain hardware.

As shown in **Errore. L'origine riferimento non è stata trovata.**, the control problem is to regulate the estimated value of the longitudinal slip ratio, λ_{act}, to a setpoint, λ_{ref}, through the variation of the motor torque demand. However, the performance of on-board electric drivetrains is affected by their torsional dynamics, mainly caused by the half-shafts [7]. For improving drivability, an active vibration controller (AVC) is included in the control structure. The AVC behaves like a virtual damper, i.e., it is a gain-scheduled proportional controller of the torsional speed of the drivetrain (see [8] for details).

IV. Models for slip ratio control

A. Plant and the simulation model

The case-study vehicle is a high performance front-wheel-drive (FWD) sport utility vehicle. The drivetrain layout, shown in , consists of one on-board electric motor per wheel. The powertrains are connected to the wheels through single-speed transmissions and half-shafts with constant velocity joints.

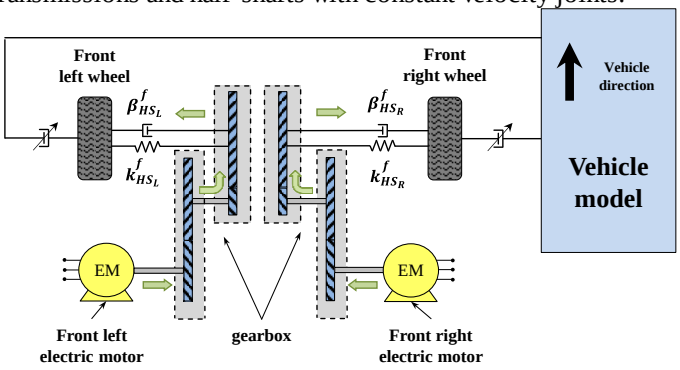

Fig. 1. Schematic drivetrain of the case study FWD electric vehicle.

The main vehicle parameters are reported in the Appendix. To evaluate the vehicle dynamics behaviour, a simulation model in the time domain has been created through the Simulink environment. The electric drivetrain dynamics have been considered by taking into account the stiffness and damping of the half-shafts. The electric motor drive has been modelled by including its torque slew rate, the air gap torque (implemented in the form of a transfer function), and the windage losses.

The system dynamics are also affected by the non-linear force vs. slip ratio characteristics of the tires, and their relaxation behaviour, variable as a function of the operating conditions of the tire. The relaxation length for each load/slip/frequency condition has been determined from the results shown in [1], in which vertical load and longitudinal slip ratio strongly influence the relaxation length.

Finally, the dynamics of the electric powertrain mounting system, especially if the drivetrain includes bushings, can affect system performance as well. All these factors can interfere with the performance of TC and ABS controllers based on electric motor torque modulation. The control system design is based on models at increasing levels of complexity:

i) a model including a steady-state linearized tire model and considering the rotating parts of the drivetrain as a rigid system (named Model 1);
ii) a model considering the transient behaviour of the tire through the concept of tire relaxation, named Model 2;
iii) a model accounting for the torsional dynamics of the half-shaft and tire relaxation, named Model 3.
iv) The model 3 including the control action of the Active Vibration Controller (AVC) (Model 4)

A wheel slip controller will be designed for each of the four models through frequency domain analysis based on gain and phase margins.

B. Model 1

$$\tau_m \dot{T}_m + T_m = T_{m,ref} \quad (2)$$

$$T_m - T_{w,f}\frac{i_g}{\eta_g} - i_g T_{roll,f} = J_{eq,1}\ddot{\theta}_m \quad (1)$$

$$2T_{f,w} - 2T_{roll,r} - T_{aer} = J_{eq,2}\ddot{\theta}_v \quad (2)$$

where

$$\eta_g = \eta_1\eta_2\,; \quad i_g = i_1 i_2; \quad (3)$$

$$J_{eq,1} = (J_1 + J_m) + \frac{i_1^2}{\eta_1}J_2 + \frac{i_g^2}{\eta_g}(J_w + J_{HS}) \quad (4)$$

$$J_{eq,2} = \left(J_{r,w} + MR_w{}^2\right) \quad (5)$$

The wheel torque, $T_{f,w}$, is a function of the longitudinal slip stiffness and the slip ratio:

$$T_{f,w} = c_\lambda \lambda R_w = c_\lambda\left(\frac{i_g\dot{\theta}_m - \dot{\theta}_v}{i_g\dot{\theta}_m}\right)R_w \quad (6)$$

The controller design is based on the transfer function $G_\lambda = \lambda/T_{m,ref}$ where λ is the slip ratio, defined in equation (7):

$$\lambda = 1 - \frac{\dot{\theta}_v}{\dot{\theta}_w} \quad (7)$$

The model has been evaluated considering the state space approach, after the linearization of the resistance forces (drag, rolling and traction force through Pacejka Magic Formula). Linearization of the forces

$$T_{w,f} = \frac{c_\lambda R_w}{i_g\dot{\theta}_{m,0}}\left(i_g\theta_m - \frac{\dot{\theta}_{v,0}}{i_g\dot{\theta}_{m,0}}\theta_v\right) + \frac{c_\lambda R_w}{i_g\dot{\theta}_{m,0}}\left(i_g\dot{\theta}_{m,0} - \dot{\theta}_{v,0}\right) \quad (8)$$

Linearized equation for rolling resistance torque:

$$T_{roll} = f_0 F_z R_w - f_2 F_z R_w^3 \left(i_g \dot{\theta}_{m,0}\right)^2 + 2 f_2 F_z R_w^3 i_g^2 \dot{\theta}_{m,0} \dot{\theta}_m \quad (9)$$

Linearized equation for aerodynamic drag resistant torque:

$$T_{aer} = \rho C_x S R_w^3 \dot{\theta}_{v,0} \dot{\theta}_v - \frac{1}{2} \rho C_{drag} S \dot{\theta}_{v,0}^2 R_w^3 \quad (10)$$

States and outputs are here reported

$$x = \left\{\dot{\theta}_m, \dot{\theta}_v, T_m\right\}^T \qquad y = \left\{\dot{\theta}_m, \dot{\theta}_v, T_m, \lambda\right\}^T \quad (11)$$

where

$$\lambda = \lambda_0 + \left\{\frac{\dot{\theta}_{v,0}}{\dot{\theta}_{w,0}^2} i_g\right\} \dot{\theta}_M + \left\{-\frac{1}{\dot{\theta}_{w,0}}\right\} \dot{\theta}_v \quad (12)$$

C. Model 2

Model 2 is characterized by the tire relaxation length. The longitudinal force $T_{d,f,w}/R_w$ of the tires is modelled using the Pacejka magic formula, including a relaxation length model for the evaluation of the transient effects, according to (13):

$$\frac{L_{tire}}{\dot{\theta}_{w,0} R_w} \dot{T}_{d,f,w} + T_{d,f,w} = T_{f,w} \quad (13)$$

Eq. 16 shows the state variables and the states:

$$x = \left\{\dot{\theta}_m, T_{d,f,w}, \dot{\theta}_v, T_m\right\}^T \qquad y = \left\{\dot{\theta}_m, T_{d,f,w}, \dot{\theta}_v, T_m, \lambda\right\}^T \quad (14)$$

D. Model 3

The complexity of the model is here increased by adding the dynamics of the half-shaft (HS). The HS is modelled as a combination of torsion spring and damper:

$$T_{HS} = \beta_{HS}\left(i_g \dot{\theta}_m - \dot{\theta}_w\right) + k_{HS}\left(i_g \theta_m - \theta_w\right) \quad (15)$$

$$x = \left\{\dot{\theta}_m, \dot{\theta}_w, \dot{\theta}_v, \theta_m, \theta_w, T_m, T_d\right\}^T \qquad y = \left\{\dot{\theta}_m, \dot{\theta}_w, \dot{\theta}_v, \theta_m, \theta_w, T_m, T_d, \lambda\right\}^T \quad (16)$$

E. Model 3 with AVC

This section shows model 3 including the active vibration control (AVC):

$$\tau_m \dot{T}_m + T_m = T_{m,ref} - K_{AVC}\left(i_g \dot{\theta}_m - \dot{\theta}_w\right) \quad (17)$$

Equation (17) includes the AVC with a constant gain $K_{AVC} = 15\ Nms/rad$. The equations of model 3, with and without the AVC, have been implemented in the state space approach for the design of the PI controller. The matrices A and B are reported in the appendix.

V. Analysis of the Vehicle Dynamics in the Frequency Domain

The slip ratio transfer function of the vehicle without TC control (the so-called "baseline vehicle") can be obtained from the equations of the four different models described in the previous section. Assuming some particular parameters for the vehicle ($\mu = 0.3$, $F_z = 6130\ N$), the frequency response of the models was analysed, given the absence of any literature about the frequency response of such powertrain. Fig. 2 plots the sensitivity of the frequency response of the same electric powertrain, modelled with increasing complexity, to a reference low slip ratio ($\lambda_{ref} = 3.3\%$). Passing from a simple model (Model 1) to a more complicated (Model 4), the response of the system changes from a first order system to a second order with a resonant peak in the region between 80 and 90 rad/s. It can also be observed that the bandwidth is between 40 and 75 rad/s.

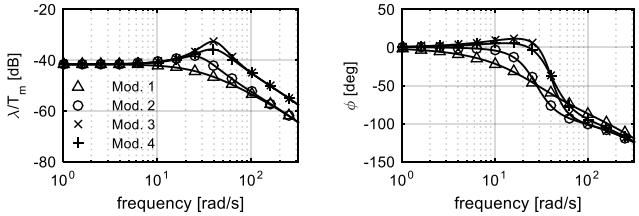

Fig. 2 – Longitudinal slip ratio frequency response evaluated for the four models at 20 km/h.

The frequency response is then evaluated for Model 4 with different vehicle speeds (Fig. 3).

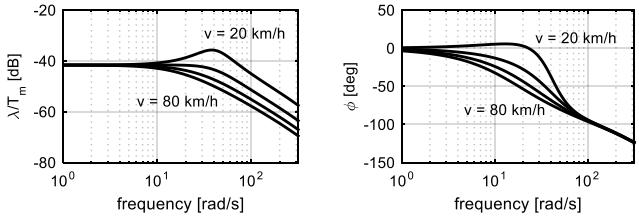

Fig. 3 - Longitudinal slip ratio frequency response evaluated for the model 4 at different vehicle speeds, starting from 20 km/h to 80 km/h with a step of 20 km/h.

VI. Control Strategies

Five different approaches for the design of the slip ratio controller generating a corrective motor torque are considered and evaluated as follows:

- a maximum transmissible torque estimation (MTTE) controller, as described in [9]
- a first order sliding mode controller (SMC), based on [10]
- a second-order sliding-mode (SOSM) control based on the suboptimal algorithm (without feedforward contribution),[10]-[13];
- PI control with gain scheduling
- an H∞ controller based on loop shaping (the general theory of loop shaping is discussed in [26][25]-[27], implemented in the form of an observer structure, suitable for the gain scheduling as function of the vehicle speed.

Condition for the activation of the controllers except for the first order sliding mode controllers are (MTTE, PID, H_∞:

$$On\ if\ \lambda > \lambda_{ref} \qquad Off\ if\ \lambda < 0.3\lambda_{ref} \quad (18)$$

A. Maximum Transmissible Torque Estimation controller

This particular controller has been developed by Hori et al [14] to avoid the problem of measuring the chassis velocity for the four wheel drive systems. Generally for vehicles characterized by just one driven axle, the vehicle speed is

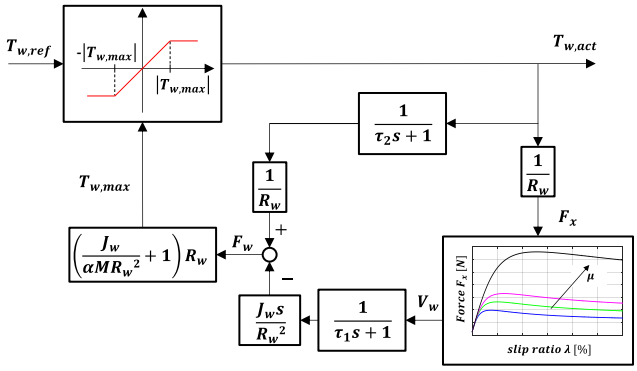

Fig. 4 – MTTE control structure

approximated using the non-driven wheels. This method is no longer suitable when the vehicle is accelerated by four-wheel drive systems thus, to overcome the problem of the speed estimation, the MTTE algorithm only make use of torque and wheel rotation as input variables to estimate the maximum transmissible torque to the road surface.

$$F_w = \frac{T_m i_g}{R_w} - \frac{J_w \dot{v}}{R_w^2} \tag{19}$$

$$\alpha = \frac{\dot{v}}{\ddot{\theta}_w} = \frac{(F_w - F_{w,r})J_w}{M(T_{w,max} - R_w F_w)R_w} \tag{20}$$

$$T_{w,max} = \left(\frac{J_w}{\alpha M R_w^2} + 1\right) R_w F_w \tag{21}$$

$$T'_{w,max} = T_{w,max} + \chi \dot{T}_{w,max} \tag{22}$$

Controller parameters, α, G, τ_1, τ_2, were selected by using an evolution strategy optimization procedure of type (1+N)-ES (for further references see [9]) to maximize the velocity of the vehicle and minimize the RMS of the slip ratio error, during a test manoeuvre performed with the non-linear simulation model.

B. *First order sliding mode controller*

In the first order sliding model controller, the control objective is to reach and remain in sliding surface $\sigma_\lambda = 0$

$$\sigma_\lambda = \lambda_{act} - \lambda_{ref} \tag{23}$$

The control law obtained by the sliding approach is composed of two terms: the first is an equivalent control term that, ideally, would keep the system in the sliding surface, as long as the system model was completely known; since this hardly happens, a switching term is added to ensure the robustness to the modelling errors [10]-[13]. Applying this design method, the sliding control law is defined as follows [10]:

$$T_{SM} = \frac{1}{b_f}\left[-\gamma_{SMC} sign(\sigma_\lambda) - F_f\right] \tag{24}$$

Where the value F_f is the feedforward contribution and γ_{SMC} is the upper bound for the uncertainty.

$$F_f = -\frac{\dot{v}}{R_w \dot{\theta}_w} - \frac{v F_x}{J_w \dot{\theta}_w^2} \tag{25}$$

$$b_f = \frac{v}{J_w R_w \dot{\theta}_w^2} \tag{26}$$

The value of γ_{SMC} should not be lower than a quantity. To show that, in spite of model disturbances, the closed loop system reaches $\sigma_\lambda = 0$ in finite time, consider the time derivative of the Lyapunov function $V(\sigma_\lambda) = \frac{1}{2}\sigma_\lambda^2$. The first sliding mode controller has been designed considering the equations of Model 1:

$$\lambda = 1 - \frac{v}{\dot{\theta}_m i_g R_w} \tag{27}$$

$$\dot{V}(s_\lambda) = \sigma_\lambda \dot{\sigma}_\lambda = \sigma_\lambda(\dot{\lambda}_{act} - \dot{\lambda}_{ref}) = \sigma_\lambda\left(-\frac{\dot{v}}{\dot{\theta}_m^2 i_g R_w} + \frac{v\ddot{\theta}_m}{\dot{\theta}_m^2 i_g R_w}\right) \leq -\gamma_{SMC}|\sigma_\lambda| \tag{28}$$

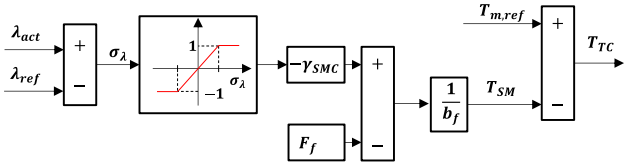

Fig. 5 – First order sliding mode control structure

C. *Sub-optimal sliding mode controller*

The main advantage of SOSM control is the ability to achieve the robustness typical of a conventional sliding-mode control while avoiding control input chattering, which can compromise vehicle comfort and drivability.

Considering a double integrator system including state variables $x_1(t)$ and $x_2(t)$

$$\begin{cases} \dot{x}_1(t) = x_2(t) \\ x_2(t) = \Phi(x,u,t) + \Gamma(x,t)v(t) \end{cases} \tag{29}$$

In a neighbourhood of the sliding manifold, $\sigma_\lambda(x,t) = y_1(t) = 0$, the uncertain terms Φ and Γ are bounded by known positive constants, i.e.

$$|\Phi(x,u,t)| \le \tilde{\Phi}$$
$$0 < \tilde{\Gamma}_1 \le \Gamma(x,t) \le \tilde{\Gamma}_2 \tag{30}$$

Depending on the relative degree between the sliding variable $\sigma_\lambda(x,t)$ and the control input, $u(t)$, $v(t)$ may present either the actual control action or its time derivative, [11]-[13]. Neglecting the losses, we obtain

$$\begin{cases} \dot{y}_1(t) = \dot{\sigma}_\lambda(x,t) = -\dfrac{\dot{v}}{\dot{\theta}_m^2 i_g R_w} + \\ \quad + \dfrac{v}{\dot{\theta}_m^2 i_g R_w}\left(\dfrac{\left(\dfrac{\eta_g T_m}{i_g} - R_w F_x\right)}{J_{eq,1}}\right) \\ \dot{y}_2(t) = \Phi(x,u,t) + \Gamma(x,t)\dot{T}_m(t) \end{cases} \tag{31}$$

The functions $\Phi(x,u,t)$ and $\Gamma(x,t)$ are reported in the appendix

$$\begin{aligned} \dot{T}_{SOSM} &= -\gamma_{SOSM}\, sign(\sigma_\lambda^*) \\ &= -\gamma_{SOSM}\, sign\left(\sigma_\lambda - \frac{1}{2}\sigma_{\lambda,M}\right) \end{aligned} \tag{32}$$

$$\gamma_{SOSM} > 2\tilde{\Phi} \tag{33}$$

The gains for the sliding mode controller were selected in order to maximize the velocity of the vehicle and minimize the RMS of the slip ratio error, during a test manoeuvre performed with the non-linear simulation model.

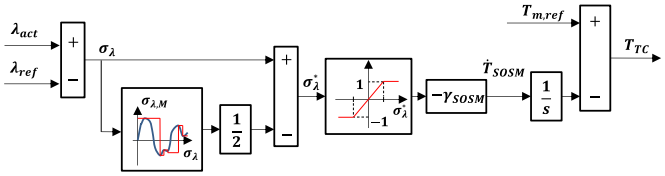

Fig. 6 – Sub-optimal sliding mode control structure

D. PI with gain scheduling

The constant gains of the conventional PI have been tuned starting from the frequency response characteristic of the open-loop system through specifications in terms of phase and gain margins, and the requirement of the closed-loop tracking bandwidth. Fig. 8 provides the integral gain and the tracking bandwidth expressed as functions of the proportional gain, for two different vehicle speed.

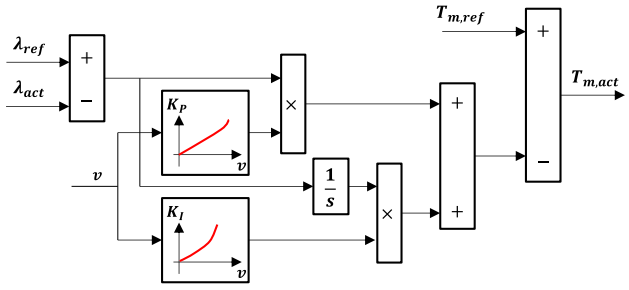

Fig. 7 – PI with gain scheduling control structure

Four points within the vehicle speed range from 20 km/h to 80 km/h are selected to grid the scheduling set and the pre-compensator is designed individually for each of these points to ensure that the controller behaves consistently at different vehicle speeds. To achieve this objective, the compensator parameters is adjusted to provide similar stability margin and cut-off frequency. In order to find the proportional and integral gains, for the required specifications of 15 dB and 60 deg, an optimization procedure has been implemented.

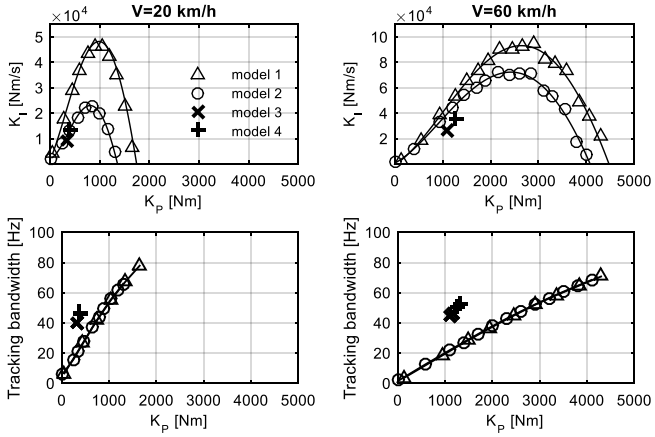

Fig. 8 – Integral gain as function of proportional gain with gain margin equal to 15±0.1 dB and phase margin 60±0.1 deg.

Grid for the gains: step of 25 for Kp and 250 Ki

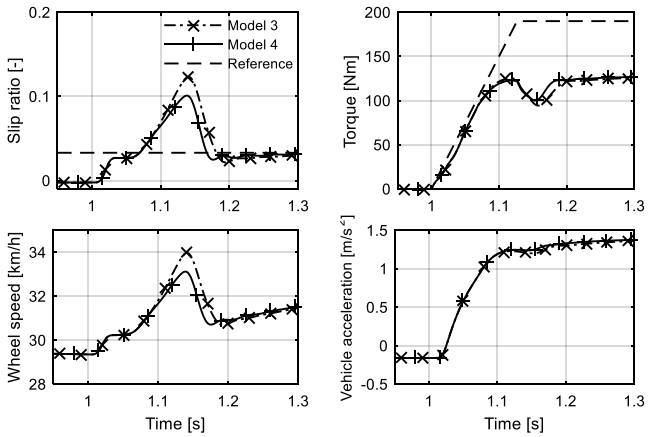

Fig. 9 – Time-domain performance comparison of PI controller with model 3 and model 3 with AVC gains.

Table 1 – Gain and phase margins sensitivity analysis.

Speed [km/h]	GM_4 [dB]	PM_4 [deg]	$GM_{4,1}$ [dB]	$PM_{4,1}$ [deg]	$GM_{4,2}$ [dB]	$PM_{4,2}$ [deg]	$GM_{4,3}$ [dB]	$PM_{4,3}$ [deg]
20	14.9	59.9	8.6	-17.5	8.1	-16.9	16.0	63.5
40	14.9	60.1	8.8	-18.6	8.6	-18.4	16.0	63.3
60	15.1	60.0	8.6	-18.4	8.6	-18.9	16.0	63.1
80	15.1	60.0	8.6	-18.8	8.5	-18.6	15.8	62.7

E. Observer based structure for H_∞ loop-shaping controllers

The mathematical formulation of the H_∞ loop shaping robust stabilization problem is provided in [26]. The structure of the H_∞ feedback controller is shown in Fig. 10. For simplicity of

notation the dependence of s the transfer functions is omitted. The plant G_λ adopted for the control system derives from model 3 and 4 (including the AVC). The H_∞ controller consists of:

i. A pre-compensator $G_{PI}(s)$ with proportional and integral gains equal to the ones used for the control structure with the only PI controller. The plant is G_λ is then multiplied by the pre-compensator and each transfer function is evaluated for different vehicle speeds (from 20 to 80 with a constant step of 20km/h)

$$W(v) = G_{PI}(v)G_\lambda(v) \tag{34}$$

ii. The actual H_∞ compensator F_s derived from the solution of the two algebraic Riccati equations reported in [26]. The order of the resulting compensator depends on the order of the system.

Table 2 - Maximum stability margin ϵ_{max} with respect to different vehicle speeds (model 3 without AVC)

Vehicle Speed [km/h]	ϵ_{max} for H_∞ controller	ϵ_{max} for H_∞ with Shaped plant	ϵ_{max} with PI for G_λ
20	0.707	0.520	0.322
40	0.707	0.516	0.326
60	0.707	0.514	0.329
80	0.707	0.514	0.331

In Table 2 and Table 3 the robustness properties of the H_∞ design are assessed through the maximum robust stability margin ϵ_{max} [26] (i.e. the maximum coprime uncertainty that can be tolerated before the system becomes unstable), for: i) the H_∞ controller designed for four vehicle speeds; ii) the H_∞ controller designed for each of the speeds, i.e., by changing the values of the vehicle speed adopted in the definition of $G_\lambda(v)$;

Table 3 - Maximum stability margin ϵ_{max} with respect to different vehicle speeds (model 4 with AVC)

Vehicle Speed [km/h]	ϵ_{max} for H_∞ controller	ϵ_{max} for H_∞ with Shaped plant	ϵ_{max} with PI for G_λ
20	0.707	0.518	0.317
40	0.707	0.514	0.329
60	0.707	0.513	0.329
80	0.707	0.512	0.329

iii) the same PI controller used for the design of the H_∞ controller. The robustness benefit of the H_∞ control design with respect to the PI is evident.

An observer/state feedback structure of the H_∞ loop shaping controller is employed in order to implement the gain scheduling scheme as a function of vehicle speed v. The transfer function $G_\lambda(s)$ is thus parameterized with the following set-up:

$$G_\lambda(v) = \begin{bmatrix} A(v) & B(v) \\ C(v) & 0 \end{bmatrix} \tag{35}$$

The compensators adopted for shaping the transfer function of the plant have been already described previously in Section… The shaped plant as a function of vehicle speed is defined as:

$$W(v) = W_{PI}(v)G_\lambda(v) = \begin{bmatrix} A_s(v) & B_s(v) \\ C_s(v) & 0 \end{bmatrix} \tag{36}$$

where the pre-compensator $W_{PI}(v)$ is scheduled by using linear interpolation between the two pre-compensators at adjacent design points h and $h+1$. In order to incorporate the gain scheduling scheme, the H_∞ loop shaping controller is implemented in the observer/state feedback form (Fig. 10):

$$\begin{cases} \dot{\lambda} = \big(A_s(v) + H_s(v)C_s(v)\big)\hat{x} + \\ +B_s(v)T_{H_\infty} + W(v)\big(\lambda_{ref} - \lambda_{act}\big) \\ T_{H_\infty} = F_s(v)\hat{\lambda} \end{cases} \tag{37}$$

Where

$$\begin{cases} H_s(v) = -Z_s^T(v)C_s^T(v) \\ F_s(v) = -B_s^T(v)[I - \varphi^{-2}I - \varphi^{-2}] \end{cases} \tag{38}$$

Z_s and F_s are the appropriate solutions to the generalized algebraic Riccati equations of the H_∞ loop shaping optimization. The observer structure of Equation (37) makes it possible to implement the H_∞ loop shaping controller directly into the gain scheduling scheme. H_s and F_s can be scheduled by linear interpolation between the adjacent design points according to (39) and (40), provided the system state-space matrices H_s and F_s vary smoothly with vehicle speed.

$$F_s(v) = \frac{v_{h+1} - v}{v_{h+1} - v_h}F_s^h + \frac{v - v_h}{v_{h+1} - v_h}F_s^{h+1} \tag{39}$$

$$H_s(v) = \frac{v_{h+1} - v}{v_{h+1} - v_h}H_s^h + \frac{v - v_h}{v_{h+1} - v_h}H_s^{h+1} \tag{40}$$

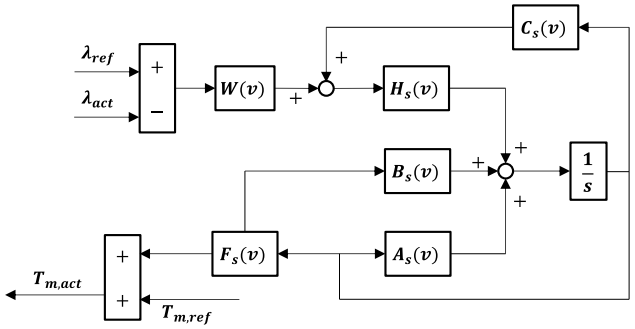

Fig. 10 - H_∞ loop-shaping controller structure

F. Friction coefficient estimation

In the results section, two different approaches will be used in order to assess the performance of the controller: i. the slip ratio reference as a constant value during the maneuver and ii) slip ratio reference implemented as a Look-up-table as a function of vertical load and estimated friction coefficient. Different estimation techniques for this parameter have been proposed in the literature, and most of them are based on the Bakker-Pacejka magic formula model. For example, [37], a procedure for the real-time estimation of μ is presented, whilst in [38], a scheme to identify different classes of roads with a Kalman filter and a least-square algorithm is presented. In [39] and [39], a recursive least-square algorithm [41] is adopted to estimate the tire-road adhesion coefficient.

A different approach is presented in [42], where an extended

Kalman filter is used to estimate the forces produced by the tires. A sliding-mode observer to estimate the longitudinal stiffness for a simplified linear tire-road interaction model was proposed in [43] and [44], whilst a dynamical tire-road interaction model with a nonlinear observer to estimate the adhesion coefficient has been proposed in [45]. In this sub-section, a first-order sliding mode observer for the online estimation of the adhesion coefficient μ is designed. The sliding mode methodology has also been adopted to design the observer since it is applicable to nonlinear systems and has good robustness properties against disturbances, modeling inaccuracy, and parameter uncertainties [46]. To design the sliding mode observer the following sliding variable has been introduced:

$$\sigma_\mu = v - \hat{v} \tag{41}$$

where $\hat{v}_x$ is an estimate of the longitudinal speed v_x. The dynamics of $\hat{v}_x$ is considered as

$$\dot{\hat{v}} = \frac{1}{M}(\Omega - Mg(f_0 + f_2 v^2) - 0.5 S\rho C_x v^2) \tag{42}$$

where

$$\Omega_{eq} = K\, sign(\sigma_\mu) \tag{43}$$

is the control signal of the sliding mode observer. By differentiating (41) one has that

$$\dot{\sigma}_\mu = \dot{v} - \dot{\hat{v}} = \frac{1}{M}\left(F_{x,f} - K_\mu\, sign(\sigma_\mu)\right) \tag{44}$$

The longitudinal $F_{x,f}$ has an upper bound such that:

$$F_{x,f} \le F_{z,f} \le \frac{Mgb - MHa\, g - 0.5 HS\rho C_x v^2}{L} \le K_\mu \tag{45}$$

The tire-road adhesion coefficient μ can be estimated by taking into account the so-called equivalent control Ω_{eq}, which is defined as the continuous control signal that maintains the system on the sliding surface $\sigma_\mu = 0$ [46]. The equivalent control can be calculated by setting the time derivative of the sliding variable $\dot{\sigma}_\mu$ equal to zero, i.e.,

$$\Omega_{eq} = F_{x,f} \tag{46}$$

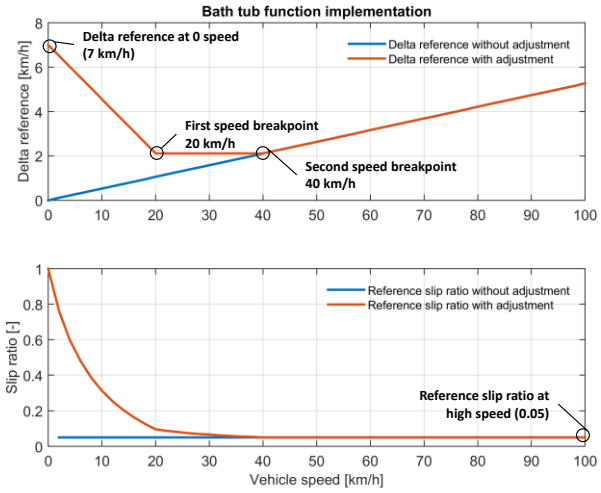

Fig. 11 – Bath tube explanation

The equivalent control must be filtered since the presence of high-frequency component. A low-pass filter is then used:

$$\Omega_{eq} = \tau\dot{\widehat{\Omega}} + \widehat{\Omega}$$
$$\widehat{\Omega} \approx \Omega_{eq} \tag{47}$$

The filter time constant should be chosen sufficiently small to preserve the slow components of the control $\widehat{\Omega}$ undistorted but large enough to eliminate the high-frequency component. The friction estimation can be then performed considering the ration between the estimated forces and the maximum traction force with $\mu = \mu^* = 1$. In formula:

$$\hat{\mu} = \frac{\widehat{\Omega}}{F_{x,f}(\lambda, F_z, \mu = 1)} \tag{48}$$

G. *Bath tube function*

At low vehicle speeds the ideal base slip is disconnected from a percentage value and connected to an absolute value. This ensures, that a vehicle can start a launch with a sufficient amount of slip – e.g.: if the vehicle speed is zero, than equals 100% slip to zero. With increasing vehicle speed, there is a smooth transition from the absolute slip value to a percentage slip value. Use of delta speed reference $\left(R_w\dot{\theta}_w - v\right)_{ref}$ instead of slip ratio reference λ_{ref}:

$$\left(R_w\dot{\theta}_w - v\right)_{ref} = \begin{cases} \left(R_w\dot{\theta}_w - v\right)_{ref,0} + \\ -\frac{v}{v_{bp,1}}\left(\left(R_w\dot{\theta}_w - v\right)_{ref,v=0} - \left(\frac{v_{bp,2}}{1-\lambda_{ref}} - v_{bp,2}\right)\right), & if\ 0 \le v \le v_{bp,1} \\ \frac{v_{bp,2}}{1-\lambda_{ref}} - v_{bp,2}, & if\ v_{bp,1} \le v < v_{bp,2} \\ \frac{v}{1-\lambda_{ref}} - v_{veh}, & if\ v_{bp,2} \le v \end{cases} \tag{49}$$

with $v_{bp,1}, v_{bp,2}$ are first and second speed breakpoints

VII. Assessment of the Performance

The performance of the yaw rate control systems is assessed through indexes related to the control action $u(t) = T_{TC}$ and the control error, $e(t) = \lambda_{act} - \lambda_{ref}$. In particular, the following

indexes are used during the relevant phases of the selected maneuvers:

- Integral of the absolute value of the control action, $IACA$ in eq.((50).
- The root-mean square value of the slip error, $RMSE$ in eq. (51)

$$IACA = \frac{1}{t_{man,fin} - t_{man,in}} \int_{t_{man,in}}^{t_{man,fin}} |T_{TC}(t)| dt \quad (50)$$

$$RMSE = \sqrt{\frac{1}{t_{man,fin} - t_{man,in}} \int_{t_{man,in}}^{t_{man,fin}} (e(t))^2 dt} \quad (51)$$

Different tests have been simulated with the Simulink vehicle model. In the following figures, three maneuvers have been selected for assessing the performance of the controllers:

Performance									
	Manoeuvre 1			Manoeuvre 2			Manoeuvre 3		
Controllers	RMS [-]	v_{final} [km/h]	IACA [Nm]	RMS [-]	v_{final} [km/h]	IACA [Nm]	RMS [-]	v_{final} [km/h]	IACA [Nm]
1st order SM	0.0541	46.6	73.83	0.0784	45.7	78.67	0.0461	64.4	83.31
SOSM	0.0799	47.5	68.69	0.1174	45.8	78.1	0.0773	69.4	70.17
MTTE	-	45.1	-	-	45.1	-	-	65.3	-
PI (mod. 4)	0.0171	48.8	61.02	0.0477	46.6	73.37	0.0134	71.7	63.81
PI+H_∞ (mod. 4)	0.0168	48.8	60.96	0.0475	46.6	73.37	0.0137	71.7	63.84
PI+H_∞ (mod. 4) + F.Est.	0.0474	48.6	62.14	0.0474	48.6	62.14	0.0503	72.0	63.25

- Manouvre 1: Tip-in acceleration test starting from 30 km/h with reference slip ratio set equal to 3.3% and road friction coefficient $\mu = 0.3$
- Manouvre 2: Tip-in acceleration test starting from 30 km/h with reference slip ratio set equal to 10% and road friction coefficient $\mu = 0.3$
- Manouvre 3: Tip-in acceleration test starting from 30 km/h with reference slip ratio set equal to 3.3% and road friction coefficient passing from 0.15 to 0.45 with a step of 0.15.

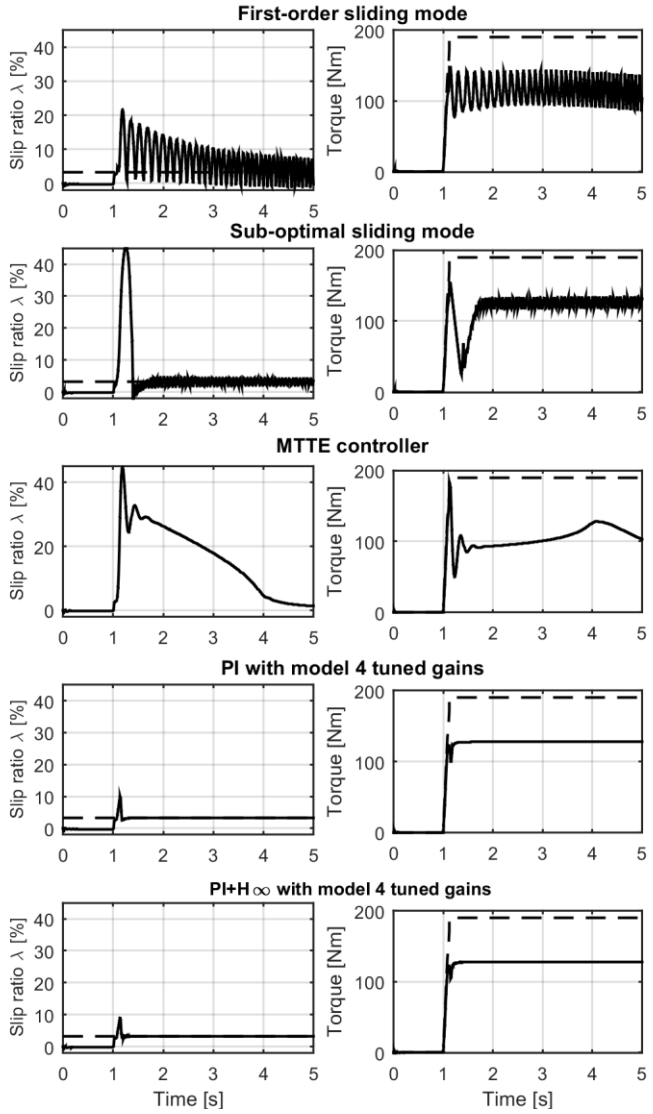

Fig. 12 – Time-domain performance of compared controllers (step torque demand, reference slip ratio 3.3%, initial speed of 30 km/h, road friction coefficient $\mu = 0.3$)

Fig. 12 shows the results in terms of slip ration and motor torque demand for the 5 controllers presented in section V.
Manovra uno: slip di riferimento pari al 3.3 % con uno step di coppia mortice pari a 180 Nm, coefficient di aderenza pari a 0.3

- Chattering nel SMC
- Il SOSM ha buone performance ma un picco iniziale piu' alto rispetto agli altri controllori
- L,MTTE funziona ma e' basato su un diverso funzionamento. Questo incide notevolmente sulle performance
-
- Tra PI e PI+H8 non c'e' sostanziale differenza. Quello che riusciamo a ridurre e' il picco iniziale.

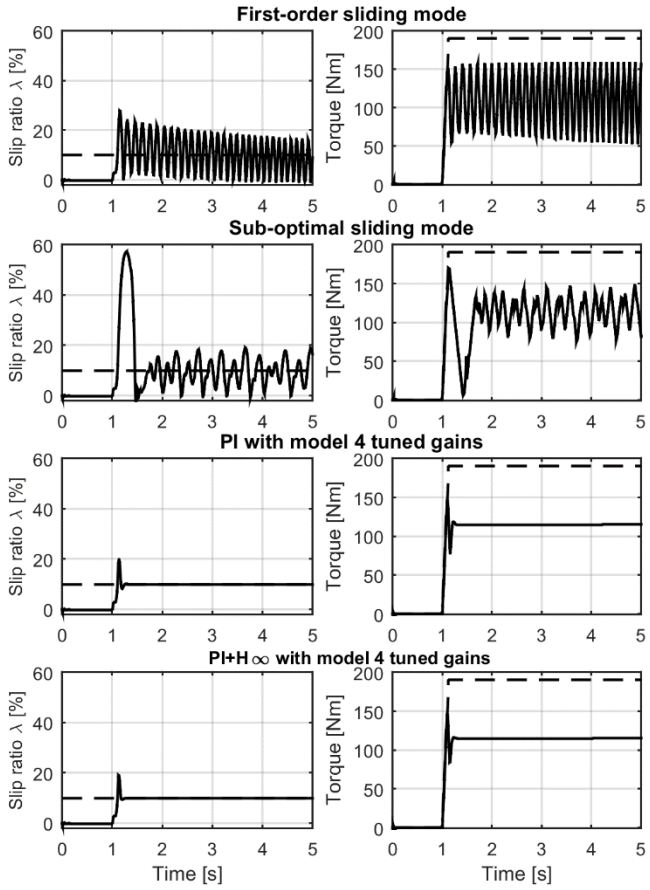

Fig. 13 – Time-domain performance of compared controllers (step torque demand, reference slip ratio 10%, initial speed of 30 km/h, road friction coefficient $\mu = 0.3$)

Seconda manovra: slip di riferimento pari al 10 % con uno step di coppia mortice pari a 180 Nm, coefficient di aderenza pari a 0.3

- Stesse considerazioni rispetto al caso precedente
- Il Sistema e' piu' robusto con il PI e il PI + H8

Terza manovra: step di coppia e slip di riferimento fisso a 3.3% ma con il coefficient di aderenza che varia tra 0.15 e 0.45 con passo di 0.15.
In questo caso le performance migliori sembrano essere quelle del PI e del PI+H8.

Quarta manovra: step di coppia e slip di riferimento variabile a seconda del coefficient di aderenza stimato. Coefficient di aderenza alle ruote che varia tra 0.15 e 0.45 con passo di 0.15.
In questo caso viene fatto solo per il PI+H8 (vedi tabella di sopra)

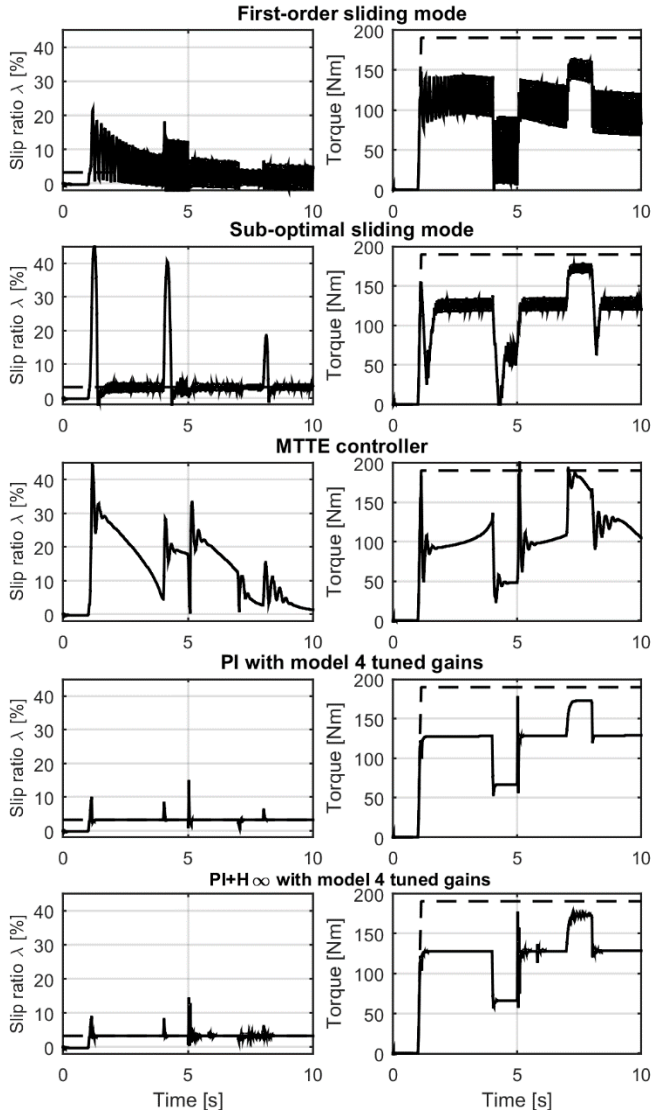

Fig. 14 – Time-domain performance of compared controllers

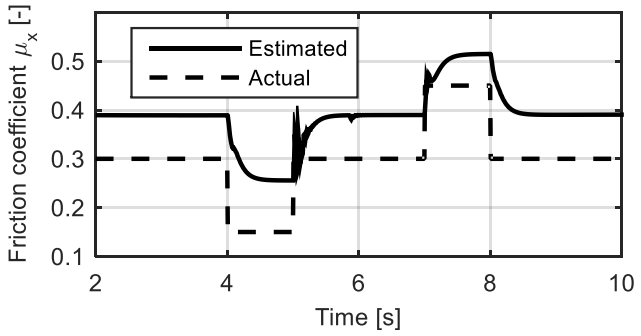

Fig. 15 – Friction coefficient estimation on Manoeuvre 3 (step torque demand, reference slip ratio 3.3%, initial speed of 30 km/h, varying road friction coefficient μ between $0.15 - 0.45$)

VIII. CONCLUSIONS

ACKNOWLEDGMENT

The research leading to these results has received funding from the European Union Seventh Framework Programme FP7/2007-2013 under grant agreements n° 605502 (PLUS-MOBY) and n° 608784 (FREE-MOBY).

REFERENCES

[1] L. De Novellis, A. Sorniotti, P. Gruber and A. Pennycott, "Comparison of Feedback Control Techniques for Torque-Vectoring Control of Fully Electric Vehicles," in *IEEE Transactions on Vehicular Technology*, vol. 63, no. 8, pp. 3612-3623, Oct. 2014.

[2] T. Goggia et al., "Integral Sliding Mode for the Torque-Vectoring Control of Fully Electric Vehicles: Theoretical Design and Experimental Assessment," in IEEE Transactions on Vehicular Technology, vol. 64, no. 5, pp. 1701-1715, May 2015.

[3] D. Yin, S. Oh and Y. Hori, "A Novel Traction Control for EV Based on Maximum Transmissible Torque Estimation," in IEEE Transactions on Industrial Electronics, vol. 56, no. 6, pp. 2086-2094, June 2009.

[4] T. A. Johansen, I. Petersen, J. Kalkkuhl and J. Ludemann, "Gain-scheduled wheel slip control in automotive brake systems," in IEEE Transactions on Control Systems Technology, vol. 11, no. 6, pp. 799-811, Nov. 2003.

[5] Vertec, Vehicle, road, tyre and electronic control system interaction – Prediction and validation of handling behaviour, EC-Contract G3RD-2002-0805, Third International Colloquim on Vehicle Tyre Road Interaction, Stuttgart, Baden-Wurttemberg, Germany, March 8, 2006.

[6] H. Beyer, "The theory of evolution strategies", Springer Verlag, 2001

[7] F. Bottiglione, A. Sorniotti, and L. Shead, "The effect of half-shaft torsion dynamics on the performance of a traction control system for electric vehicles", Proceedings of the Institution of Mechanical Engineers, Part D: Journal of Automobile Engineering September 2012 226:1145-1159.

[8] J.M. Rodriguez, R. Meneses, J. Orus, "Active vibration control for electric vehicle compliant drivetrains," Industrial Electronics Society, IECON 2013 - 39th Annual Conference of the IEEE , vol., no., pp.2590,2595, 10-13 Nov. 2013.

[9]

[10] Amodeo, M., et al., *Wheel Slip Control via Second-Order Sliding-Mode Generation*. IEEE Transactions on Intelligent Transportation Systems, 2010. 11(1): p. 122-131.

[11] G. Bartolini, "Applications of a sub-optimal discontinuous control algorithm for uncertain second order systems," Int. J. Robust Nonlin. Control, vol. 7, no. 4, pp. 299–313, Apr. 1997

[12] G. Bartolini, A. Ferrara, and E. Usai, "Chattering avoidance by secondorder sliding mode control," IEEE Trans. Autom. Control, vol. 43, no. 2, pp. 241–246, Feb. 1998

[13] G. Bartolini, A. Ferrara, A. Pisano, and E. Usai, "On the convergence properties of a 2-sliding control algorithm for non-linear uncertain systems," Int. J. Control, vol. 74, no. 7, pp. 718–731, Jan. 2001

[14] Yin, D., S. Oh, and Y. Hori, *A Novel Traction Control for EV Based on Maximum Transmissible Torque Estimation*. IEEE Transactions on Industrial Electronics, 2009. 56(6): p. 2086-2094.

[15] Ivanov, V., D. Savitski, and B. Shyrokau, *A Survey of Traction Control and Antilock Braking Systems of Full Electric Vehicles With Individually Controlled Electric Motors*. IEEE Transactions on Vehicular Technology, 2015. 64(9): p. 3878-3896.

[16] Castro, R.d., R.E. Araujo, and D. Freitas, *Wheel Slip Control of EVs Based on Sliding Mode Technique With Conditional Integrators*. IEEE Transactions on Industrial Electronics, 2013. 60(8): p. 3256-3271.

[17] Fujimoto, H., J. Amada, and K. Maeda. *Review of traction and braking control for electric vehicle*. in *2012 IEEE Vehicle Power and Propulsion Conference (VPPC)*. 2012.

[18] Guo, H., et al. *Optimal slip based traction control for electric vehicles using feedback linearization*. in *2014 International Conference on Mechatronics and Control (ICMC)*. 2014.

[19] Kuntanapreeda, S., *Super-twisting sliding-mode traction control of vehicles with tractive force observer*. Control Engineering Practice, 2015. 38: p. 26-36.

[20] Li, H.-Z., et al., *PID plus fuzzy logic method for torque control in traction control system*. International Journal of Automotive Technology, 2012. 13(3): p. 441-450.

[21] Nam, K., Y. Hori, and C. Lee, *Wheel Slip Control for Improving Traction-Ability and Energy Efficiency of a Personal Electric Vehicle*. Energies, 2015. 8(7): p. 6820-6840.

[22] Subudhi, B. and S.S. Ge, *Sliding-Mode-Observer-Based Adaptive Slip Ratio Control for Electric and Hybrid Vehicles*. IEEE Transactions on Intelligent Transportation Systems, 2012. 13(4): p. 1617-1626.

[23] Young, J.-S. and K.-J. Chen, *A Feasible Approach For The Force Control Of Traction Wheels Driven By Electric Motors*. Asian Journal of Control, 2016. 18(1): p. 112-121.

[24] Yuan, L., et al. *Model predictive slip control for electric vehicle with four in-wheel motors*. in *2015 34th Chinese Control Conference (CCC)*. 2015.

[25] S. Skogestad, I. Postlethwaite, "Multivariable Feedback Control – Analysis and Design," Wiley, 2005.

[26] D. McFarlane, K. Glover, "A loop shaping design procedure using H∞ synthesis," *IEEE Transactions on Automatic Control*, Vol. 37(6), pp. 759-769, 1992.

[27] R.A. Hyde, K. Glover, "The application of scheduled H∞ controllers to a vstol aircraft," *IEEE Transactions on Automatic Control*, Vol. 38(7), pp. 1021-1039, 1993.

[28] PATENTS

[29] Svensson, T., Joyce, J.P., *Systems and methods for wheel slip control in a vehicle*, P.N. 20150329093, 2015.

[30] Higuici, Y., Takeoka, T., *Control device of electric vehicle*, US 8615339 B2, 2013.

[31] Collins, E.G., Chuy, O., *Slip mitigation control for electric ground vehicles*, WO 2015058059 A1, 2015.

[32] Arbitmann, M., Chen, Z., Raste, T., Lauer, P., Muntu, M., Schmitz, D., *Slip-controlled braking system for electrically driven motor vehicles*, US 20140257664 A1, 2014.

[33] Enomot, H., Furuya, Y., *Vehicle control device and vehicle control method*, P.N. 20160001779, 2016.

[34] Okubo, S., Butcher, J.A., Kozarekar, S.S., *System and method for hybrid vehicle control during wheel slip events to limit generator speed*, US 9139088 B2, 2015.

[35] Iwata, T., *Traction control system for automotive vehicle and traction control method therefor*, US 5279382 A, 1994.

[36] Hrovat, D.D., Tran, M.N., Yester, J.L., Traction control for moving a vehicle from deep snow, US 5735362 A, 1998.

[37] U. Kiencke, "Real time estimation of adhesion characteristic between tyres and road," in Proc. IFAC World Congr., Sydney, Australia, 1993, vol. 1, pp. 15–18.

[38] F. Gustafsson, "Slip-based tire–road friction estimation," Automatica, vol. 33, no. 6, pp. 1087–1099, Jun. 1997.

[39] H. Lee and M. Tomizuka, "Adaptive vehicle traction force control for intelligent vehicle highway systems (IVHSs)," *IEEE Trans. Ind. Electron.*, vol. 50, no. 1, pp. 37–47, Feb. 2003.

[40] A. Ferrara and C. Vecchio, "Low vibration vehicle traction control to solve fastest acceleration/deceleration problems via second order sliding modes," in Proc. Amer. Control Conf., New York, 2007, pp. 5236–5241.

[41] L. Ljung, System Identification, Theory for the User. Englewood Cliffs, NJ: Prentice-Hall, 1999.

[42] L. R. Ray, "Nonlinear tire force estimation and road friction identification: Simulation and experiments," Automatica, vol. 33, no. 10, pp. 1819–1833, Oct. 1997.

[43] S. Drakunov, U. Özgüner, P. Dix, and B. Ashrafi, "ABS control using optimum search via sliding modes," IEEE Trans. Control Syst. Technol., vol. 3, no. 1, pp. 79–85, Mar. 1995.

[44] N. M'sirdi, A. Rabhi, L. Fridman, J. Davila, and Y. Delanne, "Second order sliding mode observer for estimation of velocities, wheel slip, radius and stiffness," in Proc. Amer. Control Conf., Minneapolis, MN, 2006, pp. 3316–3321.

[45] C. Canudas-De-Wit and R. Horowitz, "Observers for tire/road contact friction using only wheel angular velocity information," in Proc. 38th Conf. Decision Control, Phoenix, AZ, 1999, pp. 3932–3937.

[46] V. Utkin, *Sliding Modes in Control Optimization*. Berlin, Germany: Springer-Verlag, 1992.

APPENDIX

A AND B MATRICES:

$$A=\begin{bmatrix} -\frac{\beta_{HS}i_g^2}{\eta_g J_{eq,3}} & \frac{\beta_{HS}i_g^2}{\eta_g J_{eq,3}} & 0 & -\frac{k_{HS}i_g^2}{\eta_g J_{eq,3}} & \frac{k_{HS}i_g^2}{\eta_g J_{eq,3}} & \frac{1}{J_{eq,3}} & 0 \\ \frac{\beta_{HS}i_g}{\eta_g J_{eq,4}} & -\frac{\beta_{HS}}{\eta_g J_{eq,4}} & 0 & \frac{k_{HS}i_g}{\eta_g J_{eq,4}} & -\frac{k_{HS}}{\eta_g J_{eq,4}} & 0 & -\frac{1}{J_{eq,4}} \\ 0 & 0 & a_{3,3} & 0 & 0 & 0 & \frac{2}{J_{eq,5}} \\ 1 & 0 & 0 & 0 & 0 & 0 & 0 \\ 0 & 1 & 0 & 0 & 0 & 0 & 0 \\ -\frac{i_g K_{AVC}}{\tau_m} & \frac{K_{AVC}}{\tau_m} & 0 & 0 & 0 & -\frac{1}{\tau_m} & 0 \\ 0 & \frac{\dot{\theta}_{v,0}c_\lambda R_w}{\dot{\theta}_{w,0}\dot{\theta}_{v,0}\tau_d} & -\frac{c_\lambda R_w}{\dot{\theta}_{v,0}\tau_d} & 0 & 0 & 0 & -\frac{1}{\tau_d} \end{bmatrix}$$

$$B=\begin{bmatrix} 0 & 0 & 0 & 0 & 0 & 0 & 0 \\ 0 & \frac{1}{J_{eq,4}} & \frac{1}{J_{eq,4}} & 0 & 0 & 0 & 0 \\ 0 & 0 & 0 & \frac{2}{J_{eq,5}} & \frac{2}{J_{eq,5}} & \frac{1}{J_{eq,5}} & \frac{2}{J_{eq,5}} \\ 0 & 0 & 0 & 0 & 0 & 0 & 0 \\ 0 & 0 & 0 & 0 & 0 & 0 & 0 \\ \frac{1}{\tau_m} & 0 & 0 & 0 & 0 & 0 & 0 \\ 0 & 0 & 0 & 0 & 0 & 0 & \frac{1}{\tau_d} \end{bmatrix} \quad (52)$$

$$a_{3,3}=-\frac{f_0 R_w^2 Mg+2(f_2 R_w^3 Mg+\rho C_x S R_w^3)\dot{\theta}_{v,0}}{2J_{eq,5}}$$

$$J_{eq,3}=\left[(J_1+J_m)+\frac{i_1^2}{\eta_1}J_2+\frac{i_g^2}{\eta_g}\left(\frac{1}{2}J_{HS}\right)\right]$$

$$J_{eq,4}=\left(\frac{1}{2}J_{HS}+J_{f,w}\right)$$

$$J_{eq,5}=\left(2J_{r,w}+MR_w^2\right)$$

CONDITIONS FOR THE SOSM CONTROLLER:

$$\Gamma(x,t)=-\frac{\eta_g v\dot{\theta}_m^2}{J_{eq,1}\,i_g^2 R_w}$$

$$\Phi(x,u,t)=-\frac{\ddot{v}\dot{\theta}_m i_g R_w-\dot{v}\ddot{\theta}_m i_g R_w}{\left(\dot{\theta}_m i_g^* R_w\right)^2}-\frac{R_w\left[(\dot{v}F_x+v\dot{F}_x)\dot{\theta}_m^2 i_g R_w-(vF_x)i_g R_w 2\dot{\theta}_m\ddot{\theta}_m\right]}{\left(\dot{\theta}_m^2 i_g R_w J_{eq,1}\right)^2}+\frac{\eta_g}{J_{eq,1}\,i_g^2 R_w}\left[(\dot{v}T_m)\dot{\theta}_m^2-vT_m 2\dot{\theta}_m\ddot{\theta}_m\right] \quad (53)$$

VEHICLE PARAMETERS

SYMBOL	VALUE
VEHICLE PARAMETERS	
M	2500 kg
S	2.76 m^2
C_x	0.39 $[-]$
L	2.66 m
WHEEL PARAMETERS	
J_w	0.9 kgm^2
R_w	370 mm
HALF-SHAFT PARAMETERS	
β_{HS}	0.04 Nms/rad
k_{HS}	12693 Nm/rad
GEARBOX PARAMETERS	
i_g	$1/5.9$ $[-]$
i_1	$1/4.7$ $[-]$
i_2	$1/1.2$ $[-]$
MOTOR PARAMETERS	
$T_{m,max}$	200 Nm
$P_{m,max}$	80 kW
J_m	0.016 kgm^2